5-1-2011

Noninvasive MRI measures of microstructural and cerebrovascular changes during normal swine brain development

Jeff D. Winter
Hospital for Sick Children University of Toronto

Stephanie Dorner
Thornhill Research Inc.

Jelena Lukovic
Hospital for Sick Children University of Toronto

Joseph A. Fisher
University Health Network University of Toronto

Keith S. St. Lawrence
Western University, kstlawr@uwo.ca

See next page for additional authors

0031-3998/11/6905-0418
PEDIATRIC RESEARCH

Vol. 69, No. 5, 2011
Printed in U.S.A.

Noninvasive MRI Measures of Microstructural and Cerebrovascular Changes During Normal Swine Brain Development

JEFF D. WINTER, STEPHANIE DORNER, JELENA LUKOVIC, JOSEPH A. FISHER, KEITH S. ST. LAWRENCE, AND ANDREA KASSNER

Department of Physiology and Experimental Medicine [J.D.W., J.L.], The Hospital for Sick Children, Toronto, Ontario M5G 1X8, Canada; Thornhill Research Inc. [S.D.], Toronto, Ontario M5G 2E8, Canada; Departments of Anesthesiology [J.A.F.] and Medical Imaging [A.K.], University Health Network, University of Toronto, Toronto, Ontario M5S 3E2, Canada; Department of Medical Biophysics [K.S.L.], University of Western Ontario, London, Ontario N6A 5C1, Canada

ABSTRACT: The swine brain is emerging as a potentially valuable translational animal model of neurodevelopment and offers the ability to assess the impact of experimentally induced neurological disorders. The goal for this study was to characterize swine brain development using noninvasive MRI measures of microstructural and cerebrovascular changes. Thirteen pigs at various postnatal ages (2.3–43.5 kg) were imaged on a 1.5-Tesla MRI system. Microstructural changes were assessed using diffusion tensor imaging measures of mean diffusivity and fractional anisotropy. Cerebrovascular changes were assessed using arterial spin labeling measures of baseline cerebral blood flow (CBF) and the cerebrovascular reactivity (CVR) of the blood-oxygen level dependent (BOLD) MRI signal to CO_2. We found a positive logarithmic relationship for regional tissue volumes and fractional anisotropy with body weight, which is similar to the pattern reported in the developing human brain. Unlike in the maturing human brain, no consistent changes in mean diffusivity or baseline CBF with development were observed. Changes in BOLD CVR exhibited a positive logarithmic relationship with body weight, which may impact the interpretation of functional MRI results at different stages of development. This animal model can be validated by applying the same noninvasive measures in humans. **(*Pediatr Res* 69: 418–424, 2011)**

Processes of human brain development are integral to the understanding of the long-term impact of neurological disorders afflicting the immature brain. Animal models provide a means to investigate developmental processes in a controlled manner and to model the effects of disease and injury on the immature brain. Dobbing and Sands (1) proposed that the swine brain may represent an appropriate model for the immature human brain based on the timing of the brain growth spurt (rapid stages of brain growth), which is recognized as a period of increased vulnerability to injury. Additional benefits of the swine model for developmental neuroscience include similar histology, cortical folding, and gray-matter (GM)-to-white-matter (WM) ratio to humans (1). Moreover, recent advances in transgenic neural gene manipulations and the ability to model brain injury and neurologic disorders have also supported the increasing use of swine as a model for neuroscience and neurosurgical research (2,3).

Ontogeny of the brain typically focuses on structural changes during development; however, these changes may also be linked to cerebrovascular development based on the observed association between rapid stages of brain growth and increased cerebral perfusion that is believed to be required to match increased metabolic needs (4). Given that many pathologies of the immature brain involve compromised cerebral perfusion (*e.g.*, neonatal encephalopathy and intraventricular hemorrhage), there is a need to characterize both cerebrovascular and structural changes occurring in animal models of early human brain development.

MRI is emerging as the prominent modality for noninvasive assessment of morphology and microstructure in the developing human brain and offers the potential to noninvasively assess cerebrovascular development. High-resolution three-dimensional MRI provides measures of brain volume and cortical folding, whereas diffusion tensor imaging (DTI) offers the ability to track microstructural organization and composition throughout the stages of development (5–10). Cerebral blood flow (CBF) levels at different stages of development have also been measured noninvasively by arterial spin labeling (ASL), an MR technique that exploits endogenous blood water as a contrast agent (11). Another potentially important parameter, which is not well-characterized during development, is cerebrovascular reactivity (CVR), which can be assessed using MRI measures of the CBF response to a vasoactive stimulus (*e.g.* CO_2). Together, these MRI measures provide means to comprehensively assess structural and cerebrovascular development.

Received April 14, 2010; accepted November 15, 2010.
Correspondence: Andrea Kassner, Ph.D., Department of Medical Imaging, University of Toronto, Fitzgerald Building, 150 College Street, Toronto, Ontario M5S 3E2, Canada; e-mail: andrea.kassner@utoronto.ca
This study was supported by the Ontario Research Fund.

Abbreviations: ASL, arterial spin labeling; **BOLD,** blood-oxygen level dependent; **CBF,** cerebral blood flow; **CGM,** cortical gray matter; **CVR,** cerebrovascular reactivity; **CWM,** cortical white matter; **DGM,** deep gray matter; **DTI,** diffusion tensor imaging; **DWM,** deep white matter; **FA,** fractional anisotropy; **FOV,** field-of-view; **GM,** gray matter; **MD,** mean diffusivity; **MPET,** model-driven prospective end-tidal targeting; **PetCO$_2$,** end-tidal partial pressures of CO_2; **$R_{1tissue}$,** tissue longitudinal relaxation rate; **TE,** echo time; **TR,** repetition time; **WM,** white matter.

In this study, we aim to further characterize the developing swine brain as a model for translational neuroimaging research by quantifying microstructural and cerebrovascular changes during maturation *via* MRI. We present quantitative measures of brain volume changes using 3D high-resolution MRI, microstructural changes using DTI, baseline CBF, and finally, blood oxygenation level dependent (BOLD) signal changes in response to precise end-tidal (*i.e.* end exhaled) partial pressure of CO_2 ($PetCO_2$) to measure CVR in swine of various postnatal ages.

METHODS

Our institutional animal care committee approved this study and all animal procedures were conducted according to the Canadian Council on Animal Care. Thirteen 1-wk to 3-mo-old Yorkshire pigs were imaged on a 1.5-Tesla MRI scanner (General Electric Healthcare, Milwaukee, WI). An eight-channel receive-only head coil provided radiofrequency detection, and the body coil was used for radiofrequency transmission.

Animal preparation. Anesthesia was induced with an intramuscular injection of 0.2 mL/kg Akmezine and switched to 3% isoflurane for intubation and insertion of a catheter into the ear vein for a constant delivery of i.v. anesthesia (22 mg/kg/h ketamine with 1 mg/kg/h midazolam). Paralysis was maintained with pancuronium (0.2 mg/kg bolus and 1 mg/kg/h constant infusion) to assist mechanical ventilation. Animals were under anesthetic for ~2–3 h.

Anatomical imaging. High-resolution 3D T1-weighted anatomical images were acquired using a fast spoiled gradient-recalled echo sequence: echo time (TE) = 4.2 ms, repetition time (TR) = 8.46 ms, flip angle = 20°, field-of-view (FOV) = 180 mm, slab thickness = 180 mm, and matrix size = 192 × 192 × 120. DTI was performed using 25 unique diffusion-encoding directions (b = 700 s/mm^2) and one acquisition ($b \approx 0$ s/mm^2) without diffusion weighting. The DTI data were acquired using spin echo echo-planar imaging (R = 2) and the following parameters, TE = 80 ms, TR = 5.4 s, FOV = 160 mm, matrix size = 128 × 128, slices = 16, and slice thickness = 4.5 mm. Pixel-wise mean diffusivity (MD) and fractional anisotropy (FA) images were calculated from the principal eigenvalues of the diffusion tensor.

Computer-controlled gas delivery system. Cerebrovascular imaging was performed with precise control of the end-tidal partial pressures of CO_2 and O_2 using a model-driven prospective end-tidal targeting (MPET) system (RespirAct; Thornhill Research Inc., Toronto, Canada) (12) integrated with mechanical ventilation by use of a purpose-built secondary breathing circuit. Expired gases were sampled from the endotracheal tube and the continuous partial pressure of CO_2 and O_2 were digitally recorded (LabView; National Instruments Corporation, Austin, TX). Breath-by-breath $PetCO_2$ and end-tidal partial pressure of O_2 were identified from the CO_2 and O_2 partial pressure waveforms in real time using the same customizable software and confirmed manually post hoc.

Arterial spin labeling. For baseline CBF measurements, we targeted and maintained $PetCO_2$ at 40 mm Hg *via* the MPET system. ASL data were collected using single-shot gradient-echo spiral imaging using the flow-sensitive alternating inversion recovery technique (13) with a label inversion time = 1700 ms and the following imaging parameters: FOV = 160 mm, matrix size = 64 × 64, slices = 6, slice thickness = 5 mm, slice separation = 1 mm, TE = 4 ms, and TR = 3.75 s. Tissue water signal was suppressed to mitigate effects of physiological noise and motion (14), and an arterial saturation pulse was applied (850 ms postlabel) to define the label duration. Two separate acquisitions of 64 alternating "tag" and "control" image pairs were collected. Perfusion-weighted images (ΔM) were generated by successive pair-wise subtraction of tag and control images. Four proton-density (M_o) images were also acquired separately.

To account for brain tissue R_1 relaxation rate ($R_{1tissue}$) differences, a Look-Locker approach was used to collect a train of 11 low flip angle (20°) T_1-weighted images at inversion times separated by 300 ms. The inversion-recovery signal was fit to extract pixel-wise $R_{1tissue}$ values. Custom Matlab and IDL (Interactive Data Language, Research Systems, Boulder, CO) scripts were used for ASL postprocessing. The CBF was calculated from the mean of the ΔM images using the following equation:

$$\frac{\Delta M}{M_0} = -\frac{2\alpha}{\lambda} \cdot \mathrm{CBF} \cdot e^{-R_{1a} \cdot TI} \times \left[\frac{(1 - e^{-\Delta R_1 \cdot (TI - \tau)})}{\Delta R_1} + (\tau + d - TI) \right], \quad (1)$$

where α (0.85) accounts for signal decrease caused by imperfection in the background-suppression inversion pulses, λ (0.9 mL/g) is the water partition coefficient, R_{1a} (0.8 s^{-1}) is the longitudinal relaxation rate of arterial water (15), $\Delta R_1 = R_{1a} - R_{1tissue}$, TI is the inversion time (adjusted for each slice), τ (1130 ms) is the tissue transit time for newborn pigs (16), and d is the delay between the tag and arterial saturation pulses. Voxels with CBF >200 mL/100 g/min were considered to be dominated by vascular effects and removed.

BOLD CVR. BOLD imaging was performed in two separate acquisitions using single-shot gradient-echo echo-planar imaging during MPET controlled iso-oxic $PetCO_2$ cycling between 40 and 55 mm Hg. $PetCO_2$ changes were delivered in a repeated square-wave pattern with normocapnia followed by hypercapnia in 60 s steps (total = 9 minutes). Imaging parameters included: FOV = 160 mm, matrix size = 64 × 64, number of slices = 14 − 16, slice thickness = 4.5 mm, slice separation = 0.5 mm, TE = 35 ms, and TR = 2 s. Image preprocessing included spatially smoothing (Gaussian kernel full-width half-maximum = 5 mm), motion correction, and high-pass filtering using FEAT (FMRIB Expert Analysis Tool, v 5.98, FMRIB, http://www.fmrib.ox.ac.uk/fsl, Oxford University, United Kingdom). We temporally aligned the $PetCO_2$ and BOLD signals by visually estimating the delay between the $PetCO_2$ and whole-brain BOLD signal changes. Pixel-wise CVR was determined using the slope for the linear regression between the BOLD and $PetCO_2$ signals averaged between the two acquisitions. A temporal derivative was included to improve the match of the BOLD and $PetCO_2$ data on a per-voxel basis by allowing small temporal shifts to be included in the regression model.

Image analysis. Six brain regions were investigated, including cortical GM (CGM), cortical WM (CWM), deep GM (DGM), deep WM (DWM), mesencephalon, and cerebellum. The six brain regions were each segmented from the rest of the brain using a combination of automatic (FMRIB Automated Segmentation Tool, FAST) (17) and manual segmentation of the anatomical images (Fig. 1). The DTI, ASL, and BOLD-CVR parameter maps were transformed to the anatomical images *via* low resolution T1-weighted images collected at corresponding slice locations (FMRIB Linear Image Registration Tool, FLIRT) (18) and mean parameter values were extracted for each region. Limited ASL spatial coverage meant mesencephalon and cerebellum CBF estimates were not available.

Statistical analysis. Because of the uncertainty in the animals' gestational and postnatal ages, we opted to use body weight to assess developmental changes. For the analyses, body weight was the dependent variable and the following measures were independent variables: brain volume, MD, FA, CBF, and CVR. Nonparametric Spearman rho was computed for each parameter to determine body-weight dependencies for each independent variable without assuming a specific model for the relationship. Next, regression analysis determined the relationship between body weight at scan and brain volume, MD, FA, CBF, and BOLD-CVR. We compared linear, logarithmic, and exponential model functions for each parameter and determined, based on the greatest Pearson correlation coefficient (r), that the logarithmic function provided the optimal fit for the majority of brain regions for all MRI parameters investigated. In total, the logarithmic fit yielded greater r values compared with the linear model for 20 of the 28 regressions (mean r increase = 0.04 ± 0.07). Therefore, data were fit to the logarithmic function:

$$MR\ parameter = a_0 + a_1\ \mathrm{ln}(body\ weight) \quad (2)$$

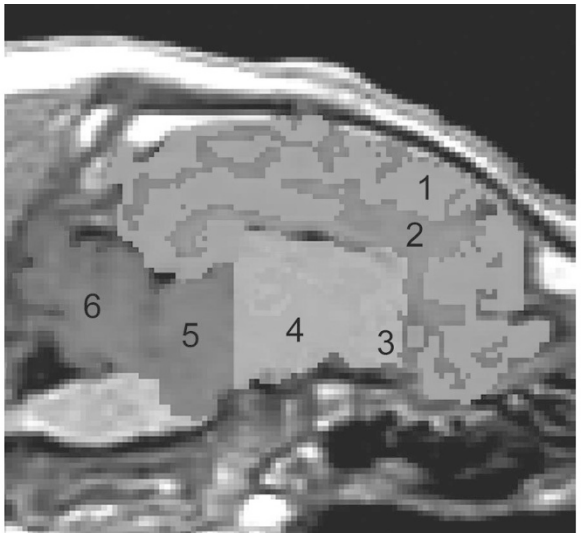

Figure 1. Saggital T1-weighted anatomical MRI with tissue regions-of-interest overlaid, including: 1, CGM; 2, CWM; 3, DGM; 4, DWM; 5, mesencephalon; and 6, cerebellum. The image was cropped to isolate the brain.

All statistical analyses were performed using SPSS v 11.0 (SPSS Inc., Chicago, IL). Results were considered statistically significant for $p < 0.05$. As this is a pilot study providing descriptive characteristics of developmental changes, the critical *p-value* was not corrected for multiple comparisons.

RESULTS

The median [range] body weight at scan for the different postnatal age groups was as follows: 1 wk old = 3.35 kg [2.3–4.4 kg] ($n = 2$); 1 mo old = 6.85 kg [5.2–9.4 kg] ($n = 4$); 2 mo old = 12.6 kg [10–14.8 kg] ($n = 3$); and 3 mo old = 24.6 kg [18.4–43.8 kg] ($n = 4$).

Nonparametric analysis demonstrated that total tissue volumes (whole brain, GM, and WM) exhibited body-weight dependencies. Follow-up parametric regression demonstrated a significant logarithmic increase in brain tissue volumes *versus* body weight (Fig. 2). Significant logarithmic relationships were also observed between brain volume and body weight for all individual brain regions investigated, except the mesencephalon (Fig. 3). Table 1 provides regression coefficients and measures of fit quality (r) for total brain volumes and individual regions.

Representative MD and FA images for 1-wk, 1-mo, 2-mo, and 3-mo-old pigs are provided in Figure 4. The DTI measurement of MD did not reveal a consistent pattern of developmental changes across the brain regions investigated (Fig. 5). Nonparametric correlation analysis revealed that MD was related to body weight in all regions except the CGM and DGM. Based on the parametric regression, a negative logarithmic relationship between MD and body weight existed in the CWM; whereas, MD in the DWM, mesencephalon and cerebellum exhibited a positive logarithmic relationship (Table 2). The FA exhibited a consistent increase with body weight across all regions after one outlier subject was removed before the analysis. The decision to remove this subject was based on poor FA map SNR, as FA values are sensitive to DTI noise levels. Parametric regressions revealed a consistent positive logarithmic relationship between FA and body weight across all six regions (Fig. 6, Table 2).

Representative baseline CBF and BOLD CVR image for four different ages are provided in Figure 7. Only one ASL data set was acquired for the 5.2 and 6.2 kg pigs (due to imaging-session time constraints), only one BOLD CVR data set was acquired for the 43.8 kg pig (due to secondary breathing circuit technical issues), and no BOLD CVR data were available for the 18.4 kg pig (due to imaging-session time constraints). A detectable BOLD response to CO_2 was not present for the smallest pig (2.3 kg) and was excluded from the regression analysis. The mean CGM CBF estimate was 52.6 ± 8.5 mL/100 g/min. No correlations existed between baseline CBF and age for either parametric or nonparametric analyses (Fig. 8, Table 3). The $R_{1tissue}$ measurements exhibited a negative linear correlation with body weight in all regions; however, because the maximum $R_{1tissue}$ difference was small (13 ± 4%), the impact on CBF estimates

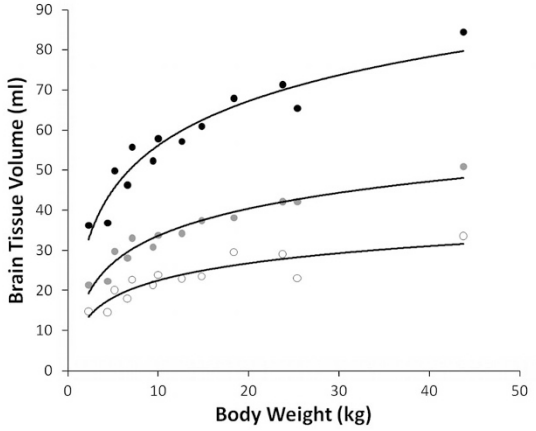

Figure 2. Log-linear regression of whole brain volume (●), total GM (◍), and total WM (○) with respect to body weight. The *solid lines* represent the log-linear regression.

Table 1. *Logarithmic regression coefficients and fit quality measures for brain tissue volume* vs *body weight (*N = *13)*

Region	Nonparametric analysis Spearman's ρ	Parametric analysis Pearson r	Model coefficients a_0	Model coefficients a_1
Whole brain	0.97*	0.96*	19.50	15.93
Total GM	0.99*	0.97*	11.08	9.79
Total WM	0.90*	0.90†	8.42	6.14
CGM	0.97*	0.96*	10.02	6.96
CWM	0.82†	0.80†	6.68	3.28
DGM	0.90*	0.92*	0.50	1.00
DWM	0.89*	0.89*	0.76	1.82
Mesencephalon	0.58‡	0.53	1.26	0.29
Cerebellum	0.94*	0.96*	0.28	2.59

* $p < 0.001$.
† $p < 0.005$.
‡ $p < 0.05$.

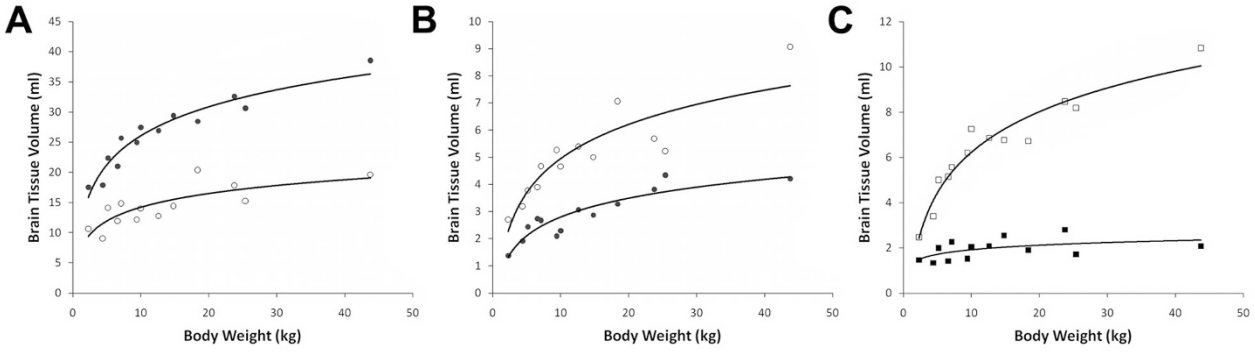

Figure 3. Log-linear regression of body weight and brain volume for each tissue region investigated: (*A*) CGM (●) and CWM (○), (*B*) DGM (●) and DWM (○), and (*C*) mesencephalon (■) and cerebellum (□).The *solid lines* represent the log-linear regression. Note that the scales for panels *A*, *B*, and *C* are different.

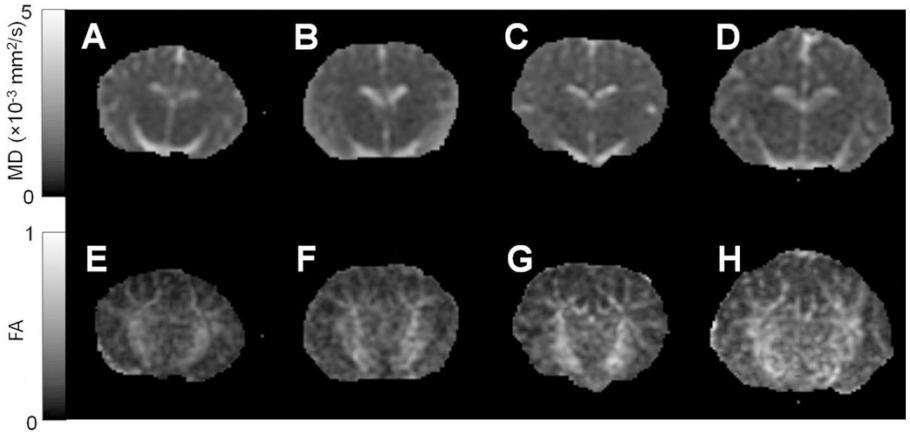

Figure 4. Representative MD maps for each age group: 1-wk-old (*A*), 1-mo-old (*B*), 2-mo-old (*C*), and 3-mo-old (*D*) pigs. Corresponding FA maps (*E–H*) are also provided.

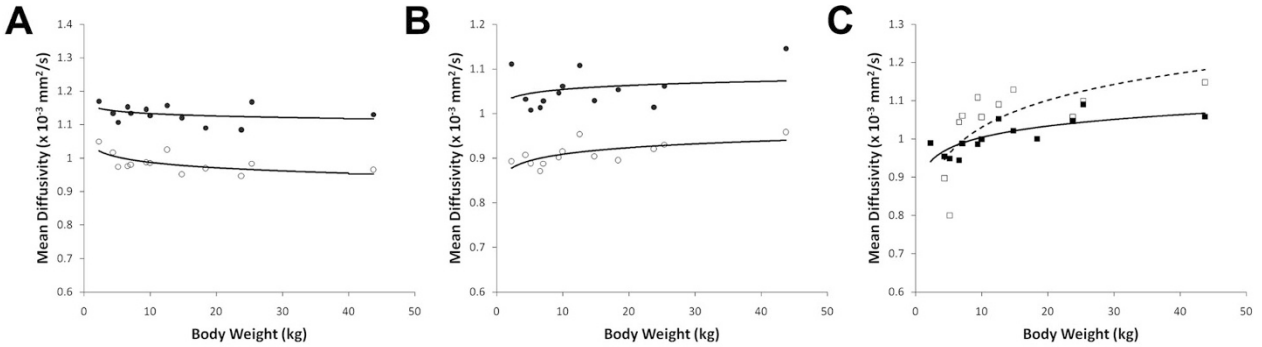

Figure 5. Relationship between body weight and MD for each tissue region investigated: (*A*) CGM (●) and CWM (○), (*B*) DGM (●) and DWM (○), and (*C*) mesencephalon (■) and cerebellum (□). The regression lines are displayed as *solid lines* for all regions except the cerebellum, which is displayed as a *dashed line*.

Table 2. *Logarithmic regression coefficients and fit quality measures for MD* (N = *13) and FA* (N = *12)* vs *body weight*

Parameter	Region	Nonparametric analysis Spearman's ρ	Parametric analysis Pearson r	Model coefficients	
				a_0	a_1
MD	CGM	−0.35	−0.39	1.166	−0.014
	CWM	−0.61*	−0.67*	1.045	−0.025
	DGM	0.29	0.24	1.025	0.013
	DWM	0.70†	0.66*	0.860	0.021
	Mesencephalon	0.85‡	0.77§	0.904	0.043
	Cerebellum	0.69†	0.55	0.92	0.058
FA	CGM	0.80§	0.87‡	0.119	0.027
	CWM	0.89‡	0.91‡	0.138	0.044
	DGM	0.58*	0.69*	0.189	0.028
	DWM	0.76†	0.80§	0.234	0.039
	Mesencephalon	0.87‡	0.91‡	0.127	0.062
	Cerebellum	0.81§	0.85‡	0.129	0.046

* $p < 0.05$.
† $p < 0.01$.
‡ $p < 0.001$.
§ $p < 0.005$.

was minimal (<4%). For BOLD CVR measurements, significant body-weight dependencies were observed for all regions except DWM, and significant logarithmic relationships with body weight were found for all six brain regions (Fig. 9, Table 3).

DISCUSSION

We investigated the swine brain as a model for early human brain development using noninvasive MRI methods performed on a clinical MRI system with reasonable scan times. Although previous studies have used invasive methods or *ex vivo* MRI techniques to characterize structural and microstructural animal brain development with greater detail (19,20), an advantage of our study is the ability to easily translate the methods and observations to clinical human studies. Unique data generated from this study include DTI parameters and ASL measures of CBF and BOLD CVR during swine brain development.

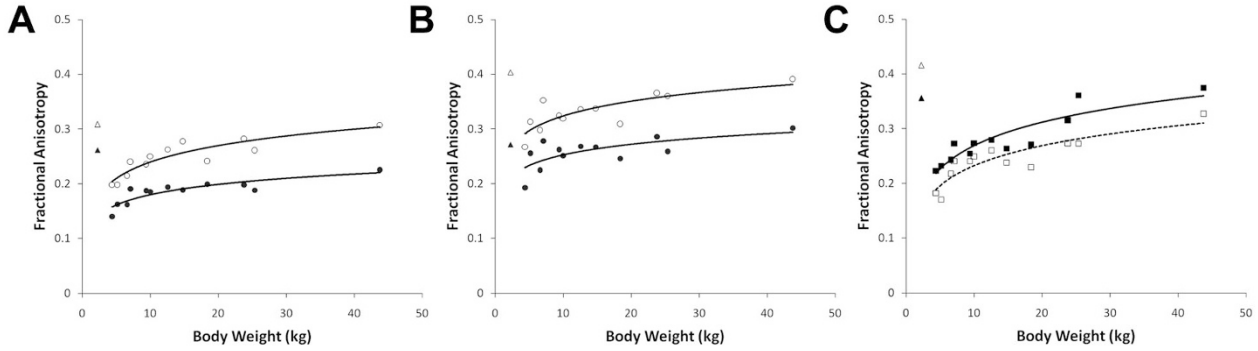

Figure 6. Log-linear regression of body weight and FA for each tissue region investigated: (*A*) CGM (●) and CWM (○), (*B*) DGM (●) and DWM (○), and (*C*) mesencephalon (■) and cerebellum (□). The regression lines are displayed as *solid lines* for all regions except the cerebellum, which is displayed as a dashed line. *Triangle symbols* represent data excluded from the analysis because of poor FA image quality.

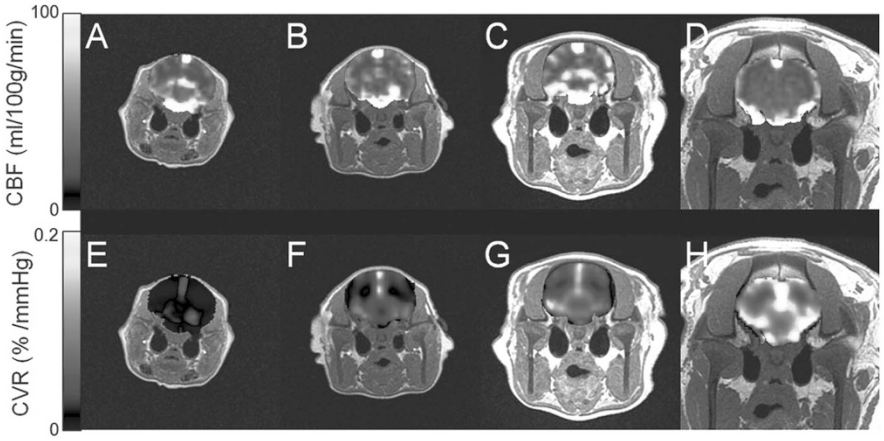

Figure 7. Representative CBF images for 1-wk-old (*A*), 1-mo-old (*B*), 2-mo-old (*C*), and 3-mo-old (*D*) pigs. Corresponding BOLD CVR images (*E–H*) are also provided.

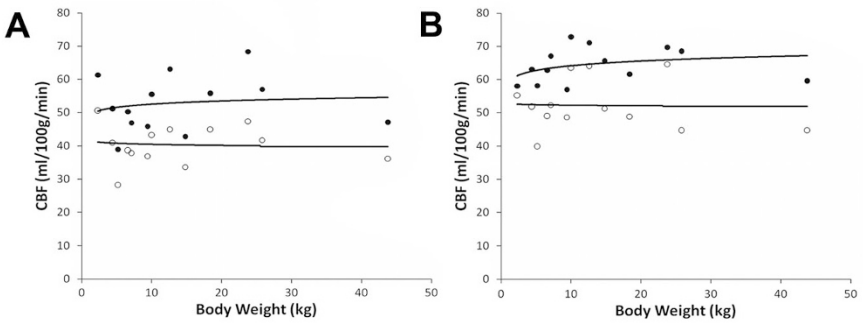

Figure 8. Relationship between body weight and CBF for each tissue region investigated: (*A*) CGM (●) and CWM (○) and (*B*) DGM (●) and DWM (○). The *solid lines* represent the log-linear regression.

For this study, we used body weight as the dependent variable to assess developmental changes instead of performing between-age-group comparisons. By doing so, we reduced the number of animals needed to characterize developmental changes and avoided the poor statistical power and need to use nonparametric statistical tests for a group-wise analysis. We consider body weight to be an appropriate surrogate for age, as we and others (21) found a smooth and continuous relationship between total brain volume and body weight. Swine brain volume changes in the current study of 1-wk to 3-mo-old pigs qualitatively match the relationship between brain volume and body weight observed in human infancy and prepubertal adolescence (22).

Consistent changes have been observed in the course of the human brain development with respect to increased FA and decreased MD with age (5–10). In the current study, we observed an increase in FA with body weight that followed a log-linear relationship. The log-linear model is often used to describe FA changes with age in the developing human brain (9,10), although models with greater complexity have been used (*e.g.* biexponential model) (8). Correspondence between swine and human FA changes during maturation is supported by previous invasive studies that suggest a similar pattern of myelination and cellular development exists in both species (21,23). That FA changes are likely attributed to myelination is based on a previous study showing that myelin sheath area was most strongly correlated with FA during development (24). However, other processes of neural development may also affect properties of water diffusion. Despite the similar pattern of FA development between our study and the developing human brain, WM FA values observed in our study (FA $\approx$ 0.2–0.4) were much lower than those reported in

Table 3. *Logarithmic regression coefficients and fit quality measures for baseline CBF (N = 13) and BOLD CVR (N = 11) vs body weight*

Parameter	Region	Nonparametric analysis Spearman's ρ	Parametric analysis	Model coefficients a_0	Model coefficients a_1
Baseline CBF	CGM	0.225	0.13	49.39	1.376
	CWM	0.11	−0.06	41.55	−0.458
	DGM	0.36	0.32	59.34	2.079
	DWM	−0.13	0.00	52.78	−0.205
BOLD CVR	CGM	0.79*	0.87†	−0.0143	0.0297
	CWM	0.75‡	0.83*	−0.0061	0.0237
	DGM	0.66§	0.79*	−0.0116	0.0288
	DWM	0.54	0.73§	−0.0040	0.0240
	Mesencephalon	0.76‡	0.83*	−0.0194	0.0347
	Cerebellum	0.85*	0.86*	−0.0231	0.0401

* $p < 0.005$.
† $p < 0.001$.
‡ $p < 0.01$.
§ $p < 0.05$.

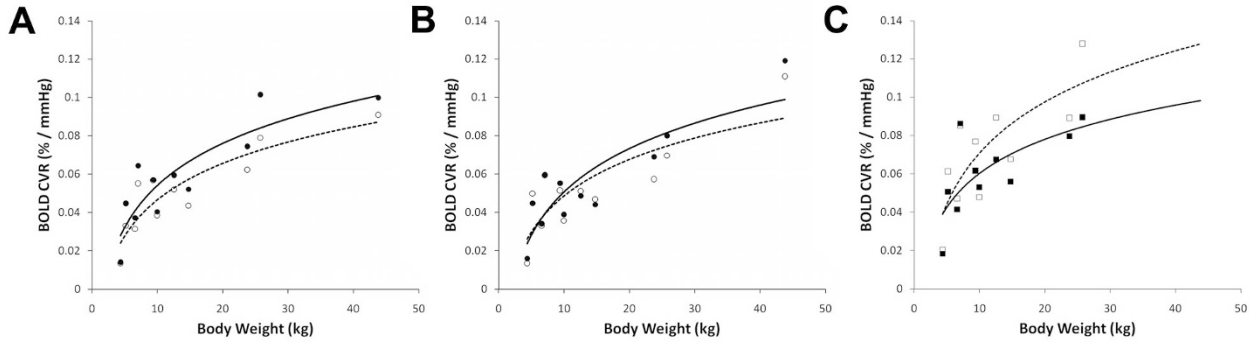

Figure 9. Relationship between body weight and the BOLD CVR for each tissue region investigated: (*A*) CGM (●) and CWM (○), (*B*) DGM (●) and DWM (○), and (*C*) mesencephalon (■) and cerebellum (□). The *solid lines* represent the log-linear regression for GM regions, and the *dashed lines* represent the log-linear regression for WM regions.

humans (<2 y old, FA ≈ 0.4–0.6) (5). This may be related to between-species differences in WM microstructure, as well as experimental factors such as increased partial volume effects in the smaller pig brain.

The small and inconsistent MD changes observed during swine brain development were unexpected as studies of human brain development observed considerable MD decreases with age (6). This discrepancy between MD trends observed in pigs *versus* that in humans is most likely due to between-species differences in the timing of brain water content changes. First, MD values in the current study were lower than values reported in the immature human brain (8) and MD in newborn pigs (25) is similar to the adult human brain. Second, water content of the human brain increases rapidly after birth (22), whereas this period of rapid water content increase occurs primarily during the prenatal period of pig brain development (26). Together, these observations suggest MD changes during swine brain development occur prenatally.

A key component of brain development is the concomitant increase in CBF during periods of rapid brain development. In humans, CBF peaks at approximately the age of 2 y, with a second smaller peak around puberty (11,27). The early phase of rapid CBF increase is mirrored by changes in glucose utilization (28) and increases in the total cell count (22). In contrast, our study failed to observe any significant changes in ASL-based measures of CBF in the 1-wk to 3-mo-old pig brain. This observation is consistent with a previous microsphere study that compared CBF in young (1–2 wk old) and older (6–8 mo old) pigs anesthetized with pentobarbitol (29). However, a more recent study measuring CBF *via* microsphere infusion demonstrated increased CBF in juvenile pigs (4–10 wk old) pigs compared with younger pigs (1–2 wk old) anesthetized with fentanyl (30). It is possible that different anesthetic combinations or CBF measurement methods could account for these inconsistent results. In the current study, use of ketamine, which tends to decrease CBF (31), and the duration of anesthesia may have obscured any CBF changes related to brain development.

One aspect of brain development that has received limited attention is the CBF reserve. Despite not observing any increases in baseline CBF, BOLD CVR increased significantly during maturation, which mirrored changes observed in brain volume and FA. These developmental changes in BOLD CVR are in contrast to a previous microsphere study that failed to observe differences in the CBF response to CO_2 between young (1–2 wk) and adult (6–10 mo) pigs (32). Our results also differ from another microsphere study that suggested that CO_2 reactivity is depressed for the first week of life, but quickly reaches adult levels between 1 wk old and 1 mo old (33). A major distinction between the current study and the cited studies is the CBF measurement approach. The BOLD signal response to CO_2 used in the current study is an indirect measure of CBF based on deoxyhemoglobin concentration changes and may also be influenced by metabolism, cerebral blood volume, and hematocrit levels. Therefore, BOLD CVR changes we observed may be more representative of overall hemodynamic and metabolic de-

velopment, including factors such as the cerebral metabolic rate of O_2. Evidence for the complex interplay between the hemodynamic and metabolic changes during human brain development is provided by the absence or negative BOLD response to visual stimulation observed in neonates (34). Results of our current study have implications for the interpretation functional MRI studies different stages of development (35).

In summary, we have further characterized the complex development processes of swine brain development using noninvasive MRI techniques that can be easily translated to the developing human brain. We found that increases in brain tissue volume and FA mirror changes observed during human brain development; however, unlike the human brain, we failed to observe substantial MD decreases. Despite the lack of maturation-related baseline CBF changes in the current study, we observed significant changes in the BOLD response to CO_2 that point to rapid changes in the metabolic and hemodynamic status during early swine brain development. The lack of MD and CBF changes in the swine brain may limit its suitability as a model for some aspects of neurodevelopment. However, for certain applications, such as morphological and DTI measures of anisotropy, future investigations of brain injury and associated neurodevelopmental sequelae in the swine brain may provide inferences into neurological disorders affecting the immature human brain.

Acknowledgments. The authors thank the assistance provided by Garry Detzler, Ruth Lanius, Marvin Estrada, and Karen Holowaty.

REFERENCES

1. Dobbing J, Sands J 1979 Comparative aspects of the brain growth spurt. Early Hum Dev 3:79–83
2. Tanaka Y, Imai H, Konno K, Miyagishima T, Kubota C, Puentes S, Aoki T, Hata H, Takata K, Yoshimoto Y, Saito N 2008 Experimental model of lacunar infarction in the gyrencephalic brain of the miniature pig: neurological assessment and histological, immunohistochemical, and physiological evaluation of dynamic corticospinal tract deformation. Stroke 39:205–212
3. Lind NM, Moustgaard A, Jelsing J, Vajta G, Cumming P, Hansen AK 2007 The use of pigs in neuroscience: modeling brain disorders. Neurosci Biobehav Rev 31:728–751
4. Epstein HT 1999 Stages of increased cerebral blood flow accompany stages of rapid brain growth. Brain Dev 21:535–539
5. Gao W, Lin W, Chen Y, Gerig G, Smith JK, Jewells V, Gilmore JH 2009 Temporal and spatial development of axonal maturation and myelination of white matter in the developing brain. AJNR Am J Neuroradiol 30:290–296
6. Cascio CJ, Gerig G, Piven J 2007 Diffusion tensor imaging: Application to the study of the developing brain. J Am Acad Child Adolesc Psychiatry 46:213–223
7. Hermoye L, Saint-Martin C, Cosnard G, Lee SK, Kim J, Nassogne MC, Menten R, Clapuyt P, Donohue PK, Hua K, Wakana S, Jiang H, van Zijl PC, Mori S 2006 Pediatric diffusion tensor imaging: normal database and observation of the white matter maturation in early childhood. Neuroimage 29:493–504
8. Mukherjee P, Miller JH, Shimony JS, Conturo TE, Lee BC, Almli CR, McKinstry RC 2001 Normal brain maturation during childhood: developmental trends characterized with diffusion-tensor MR imaging. Radiology 221:349–358
9. Löbel U, Sedlacik J, Gullmar D, Kaiser WA, Reichenbach JR, Mentzel HJ 2009 Diffusion tensor imaging: the normal evolution of ADC, RA, FA, and eigenvalues studied in multiple anatomical regions of the brain. Neuroradiology 51:253–263
10. Trivedi R, Agarwal S, Rathore RK, Saksena S, Tripathi RP, Malik GK, Pandey CM, Gupta RK 2009 Understanding development and lateralization of major cerebral fiber bundles in pediatric population through quantitative diffusion tensor tractography. Pediatr Res 66:636–641
11. Biagi L, Abbruzzese A, Bianchi MC, Alsop DC, Del Guerra A, Tosetti M 2007 Age dependence of cerebral perfusion assessed by magnetic resonance continuous arterial spin labeling. J Magn Reson Imaging 25:696–702
12. Slessarev M, Han J, Mardimae A, Prisman E, Preiss D, Volgyesi G, Ansel C, Duffin J, Fisher JA 2007 Prospective targeting and control of end-tidal CO2 and O2 concentrations. J Physiol 581:1207–1219
13. St Lawrence KS, Frank JA, Bandettini PA, Ye FQ 2005 Noise reduction in multi-slice arterial spin tagging imaging. Magn Reson Med 53:735–738
14. Ye FQ, Frank JA, Weinberger DR, McLaughlin AC 2000 Noise reduction in 3D perfusion imaging by attenuating the static signal in arterial spin tagging (ASSIST). Magn Reson Med 44:92–100
15. Ye FQ, Mattay VS, Jezzard P, Frank JA, Weinberger DR, McLaughlin AC 1997 Correction for vascular artifacts in cerebral blood flow values measured by using arterial spin tagging techniques. Magn Reson Med 37:226–235
16. Koziak AM, Winter J, Lee TY, Thompson RT, St Lawrence KS 2008 Validation study of a pulsed arterial spin labeling technique by comparison to perfusion computed tomography. Magn Reson Imaging 26:543–553
17. Zhang Y, Brady M, Smith S 2001 Segmentation of brain MR images through a hidden Markov random field model and the expectation-maximization algorithm. IEEE Trans Med Imaging 20:45–57
18. Jenkinson M, Smith S 2001 A global optimisation method for robust affine registration of brain images. Med Image Anal 5:143–156
19. Huang H, Yamamoto A, Hossain MA, Younes L, Mori S 2008 Quantitative cortical mapping of fractional anisotropy in developing rat brains. J Neurosci 28:1427–1433
20. D'Arceuil H, Liu C, Levitt P, Thompson B, Kosofsky B, de Crespigny A 2008 Three-dimensional high-resolution diffusion tensor imaging and tractography of the developing rabbit brain. Dev Neurosci 30:262–275
21. Pond WG, Boleman SL, Fiorotto ML, Ho H, Knabe DA, Mersmann HJ, Savell JW, Su DR 2000 Perinatal ontogeny of brain growth in the domestic pig. Proc Soc Exp Biol Med 223:102–108
22. Dobbing J, Sands J 1973 Quantitative growth and development of human brain. Arch Dis Child 48:757–767
23. Jelsing J, Nielsen R, Olsen AK, Grand N, Hemmingsen R, Pakkenberg B 2006 The postnatal development of neocortical neurons and glial cells in the Gottingen minipig and the domestic pig brain. J Exp Biol 209:1454–1462
24. Jito J, Nakasu S, Ito R, Fukami T, Morikawa S, Inubushi T 2008 Maturational changes in diffusion anisotropy in the rat corpus callosum: comparison with quantitative histological evaluation. J Magn Reson Imaging 28:847–854
25. Winter JD, Tichauer KM, Gelman N, Thompson RT, Lee TY, St Lawrence K 2009 Changes in cerebral oxygen consumption and high-energy phosphates during early recovery in hypoxic-ischemic piglets: a combined near-infrared and magnetic resonance spectroscopy study. Pediatr Res 65:181–187
26. Dickerson JW, Dobbing J 1967 Prenatal and postnatal growth and development of the central nervous system of the pig. Proc R Soc Lond B Biol Sci 166:384–395
27. Wintermark M, Lepori D, Cotting J, Roulet E, van Melle G, Meuli R, Maeder P, Regli L, Verdun FR, Deonna T, Schnyder P, Gudinchet F 2004 Brain perfusion in children: evolution with age assessed by quantitative perfusion computed tomography. Pediatrics 113:1642–1652
28. Chugani HT, Phelps ME, Mazziotta JC 1987 Positron emission tomography study of human brain functional development. Ann Neurol 22:487–497
29. Ichord RN, Kirsch JR, Helfaer MA, Haun S, Traystman RJ 1991 Age-related differences in recovery of blood flow and metabolism after cerebral ischemia in swine. Stroke 22:626–634
30. Nomura F, Forbess JM, Jonas RA, Hiramatsu T, du Plessis AJ, Walter G, Stromski ME, Holtzman DH 1996 Influence of age on cerebral recovery after deep hypothermic circulatory arrest in piglets. Ann Thorac Surg 62:115–122
31. Akeson J, Bjorkman S, Messeter K, Rosen I 1993 Low-dose midazolam antagonizes cerebral metabolic stimulation by ketamine in the pig. Acta Anaesthesiol Scand 37:525–531
32. Helfaer MA, Kirsch JR, Haun SE, Koehler RC, Traystman RJ 1991 Age-related cerebrovascular reactivity to CO2 after cerebral ischemia in swine. Am J Physiol 260:H1482–H1488
33. Haaland K, Karlsson B, Skovlund E, Lagercrantz H, Thoresen M 1995 Postnatal development of the cerebral blood flow velocity response to changes in CO2 and mean arterial blood pressure in the piglet. Acta Paediatr 84:1414–1420
34. Martin E, Joeri P, Loenneker T, Ekatodramis D, Vitacco D, Hennig J, Marcar VL 1999 Visual processing in infants and children studied using functional MRI. Pediatr Res 46:135–140
35. Fang M, Li J, Rudd JA, Wai SM, Yew JC, Yew DT 2006 fMRI mapping of cortical centers following visual stimulation in postnatal pigs of different ages. Life Sci 78:1197–1201